Proceedings of the 1992 IEEE/RSJ International Conference on Intelligent Robots and Systems Raleigh, NC July 7-10, 1992

MOBILITY AND MANIPULATION OF A LIGHT-WEIGHT SPACE ROBOT

Yangsheng Xu, Ben Brown, Shigeru Aoki, Takeo Kanade
The Robotics Institute
Carnegie Mellon University
Pittsburgh, Pennsylvania 15213

Abstract

We have developed a light-weight space manipulator, *Self-Mobile Space Manipulator (SM^2)*, in the Robotics Institute at Carnegie Mellon University. SM^2 is a 7-degree-of-freedom (DOF), 1/3-scale, laboratory version of a robot designed to walk on the trusswork and other exterior surfaces of Space Station Freedom, and to perform manipulation tasks that are required for inspection, maintenance, and construction. Combining the mobility and manipulation functions in one body as a mobile manipulator, SM^2 is capable of routine tasks such as inspection, parts transportation, object lighting, and simple assembly procedures. The system will provide assistance to astronauts and greatly reduce the need for astronaut extra-vehicular activity (EVA). This paper discusses the robot hardware development, gravity compensation system, control structure and teleoperation functions of the SM^2 system, and demonstrates its capabilities of locomotion and manipulation in space applications.

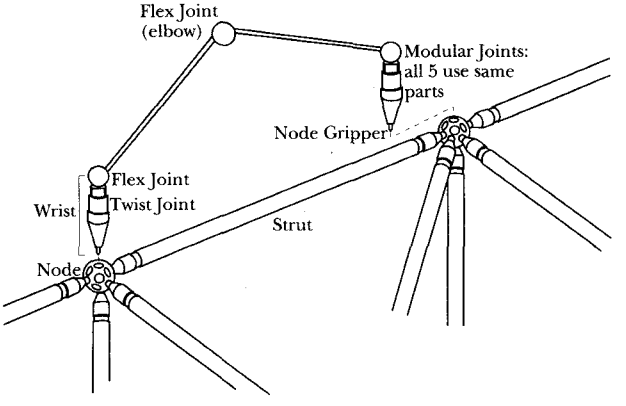

Figure 1: Basic 5-joint robot walker and Space Station trusswork.

1 Introduction

Robotic technology is beneficial for space exploration in various ways. Because of the inhospitable environment in space, the use of robots can minimize the risk that astronauts may face. The use of robots can reduce the astronaut EVA time and thus increase the productivity of the mission. Robots can provide high playload capacity and may be used on the experiments that are sensitive to human contamination. Using robots in place of humans reduces the need for human support facilities and thereby reduces the cost of space exploration.

In the Robotics Institute at Carnegie Mellon, we are developing a light-weight and low-cost robot that provides independent mobility on the Space Station exterior and at the same time is capable of accomplishing manipulation tasks. We call this robot the Self-Mobile Space Manipulator, or SM^2.

In the first phase of the project, we focused on developing the robot concept, designing the robot hardware, establishing a zero-gravity compensation testbed and developing control software for the locomotion experiments. The second phase was to develop robot manipulation capability by extending the robot hardware, implementing a teleoperated control station, and refining the gravity compensation testbed required for the tasks. In this paper we report the research and development effort in these two phases. More detailed information on the first phase is given in [1].

2 Mobility Function

2.1 Basic Concept

To achieve the mobility function of the robot on the Space Station trusswork, we developed a robot walker of minimum size and complexity. As shown in Figure 1, the robot includes five rotational joints, two slender links, and *node grippers* at both ends that enable it to attach itself

0-7803-0737-2/92$03.00 1992©IEEE

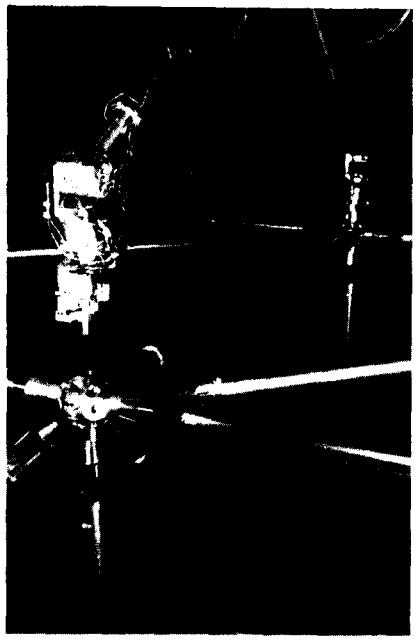

Figure 2: Photograph of SM^2 walking on the laboratory trusswork.

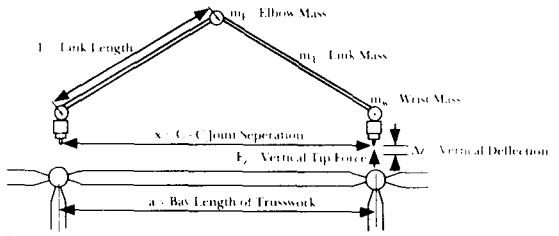

Parameter	Formula	Full Size	1/3 Size
Bay Length	a	5.00m	1.67m
Link Length	L	2.91m	0.97m
Link Tube Dimensions (OD x wall thickness)[1]		51mm x 1.0mm	19mm x 0.7mm
Link Mass[2]	m_L	1.23kg	0.11kg
Wrist Mass*	m_W	14kg	14kg
Tip Stiffness (@ x=21)[2]	$k=3EI/(2L)^3$	55.6N/m	55.4N/m
Joint Torque, peak[3]	T	41.1N-m	13.7N-m
Tip Force @ Max Joint Torque[3]	F_z	9.0N	9.0N
Tip Deflection @ Max Joint Torque[3]	$\Delta z=T(2L)^2/3EI$	148mm	148mm
Lowest Natural Frequency (@ x=21)[4]	$\omega_N=\sqrt{(k/m_W)}$	2.20 rad/sec	2.19 rad/sec
Joint Speed, max[3]	$\dot{\theta}$	1.93 rad/sec	5.8rad/sec
Step Time (nominal for 180° step)	t_{180}	20sec	6.7sec

* Estimated for self-contained robot with auxiliary manipulators.
1 Link crossectional dimensions were scaled to maintain proportional outside diameters and equal linear stiffness at the tip
2 Based on 6061-T6 aluminum: 2.8 g/cm3 density, 68,900N/mm2 elastic modulus
3 Based on 100:1 joint ratio
4 Assuming point mass at tip, all robot joints locked

Figure 3: Scaled parameters for the full-size hypothetical and 1/3-scale laboratory robot.

to threaded holes in the truss nodes or other regular structure. Walking is accomplished by alternate grasping and releasing of the nodes by the grippers, and swinging of the feet from one node to the next. During each walking step, one end of the robot releases from a node, swings 90 or 180 degrees to a desired node location, and reattaches to that node. Using such steps with alternate feet, SM^2 can move to any node on the exterior of the truss.

In order to perform realistic experiments in the laboratory, we designed and built a 1/3-size laboratory robot based on a hypothetical, full-size, self-contained robot to be used on the Space Station. Figure 2 is a photograph of SM^2 walking on the laboratory truss. We used scaling rules to keep the dynamic parameters (masses, stiffnesses, natural frequencies, linear speeds) of the scaled-down robot similar to those of the hypothetical one. Overall dimensions of the truss and robot were reduced to 1/3, while local dimensions (truss nodes, joints and grippers) were kept equal. This allows the testbed to be used in an average size laboratory, while mechanisms are not unworkably small.

2.2 Robot Mechanism

Some basic parameters of the full-size and 1/3 scale designs are shown in Figure 3. Step time (the time for the robot to swing through a 180-degree arc) was set to 20 sec for full scale, 6.7 sec for 1/3 scale; this was judged to be appropriate for safety and reasonable travel speed and energy efficiency. At both scales, the lowest structural frequency is designed to be 2.2 rad/sec (0.35 Hz), and the tip deflects 148 mm (5.8 in) under maximum joint torque while producing 9.0 N (2.0 lb) of force. Thus, the robot is highly flexible and generates relatively small forces at the tip. These characteristics dictate the kind of tasks for which SM^2 is suited, and highlight the need for controls that avoid exciting vibrations in the structure.

To simplify repairs to the robot and minimize the required inventory of parts, SM^2 was designed with five compact, modular, self-contained joints. Each joint contains a rare-earth-magnet DC motor; harmonic-drive speed reducer (60:1 or 100:1 ratio); and optical encoder on the motor shaft to measure joint angle, as shown in Figure 4. The motors and drive components were selected and arranged to give maximum power and torque in a small, light-weight package.

The node gripper was designed to anchor the robot firmly to the nodes since the robot's base of support shifts from one end to the other during walking. The node gripper (Figure 5) includes a motor-driven screw that engages the threaded holes in the nodes; and a cam mechanism that draws the gripper against the node with 1800 N (400 lb) of force to prevent twisting or rocking on the node, which would disturb the robot's frame of reference. A gap-sensing button and motor-current sensor permit automatic control of the gripping and ungripping cycles.

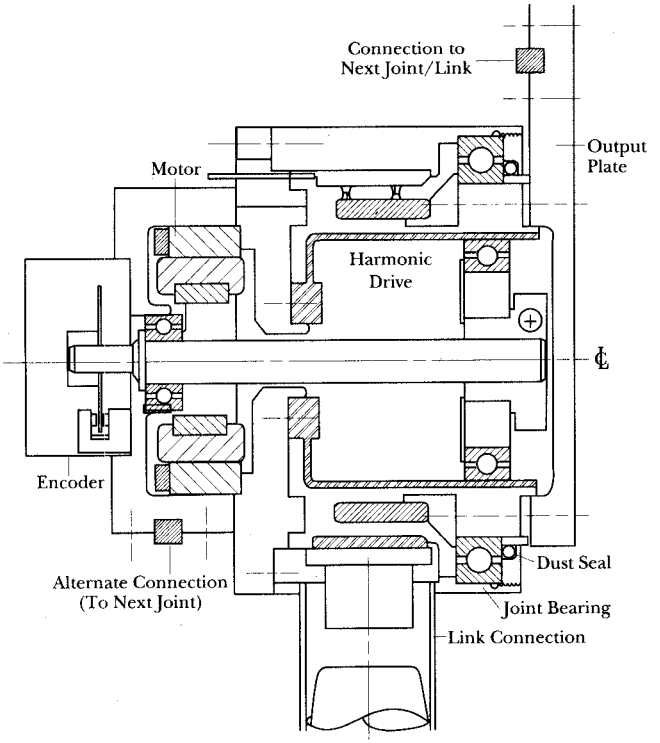

Figure 4: Each modular joint contains a DC motor, harmonic drive reducer and position sensor.

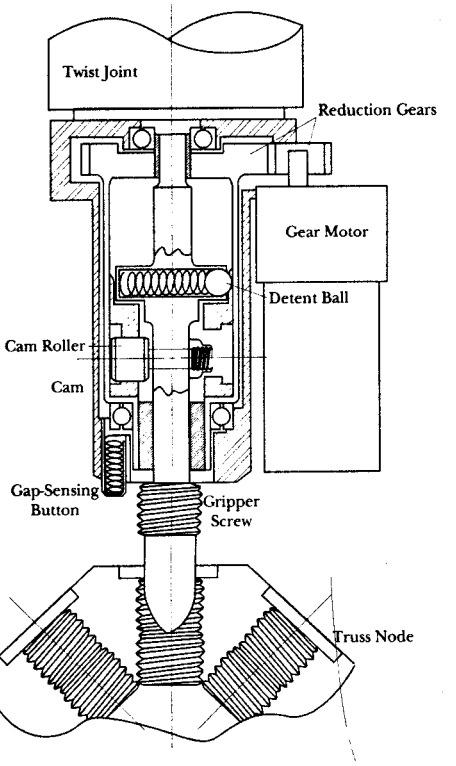

Figure 5: The node gripper has a motorized screw and a cam mechanism to generate the 1800 N (400 lb) hold-down force.

2.3 Gravity Compensation System

The absence of gravitational forces in orbit has a dramatic effect on the design and operation of robots. To permit realistic testing on Earth, we developed a gravity compensation (GC) system that balances the significant gravitational effects on the robot. The system, shown in Figure 6 includes a passive, vertical counterweight system, and an actively controlled, horizontal system. The vertical system comprises a counterweight mechanism, and a series of pulleys and cables that provide a constant upward force to balance the weight of the robot. Because of its 10:1 ratio, the counterweight mechanism increases the inertia of the system by only 10% in the vertical direction. (A 1:1 ratio would double the inertia.) The support cable is routed through idler pulleys in a manner that decouples horizontal and vertical motions.

The overhead carriage is actively controlled along the two horizontal axes to maintain the support point directly above the robot. A video camera and an automatic vision system, tracking an LED mounted above the robot, generate position error signals used for servocontrol of x-y positioning motors. GC control is independent of the robot control system.

2.4 Controls

2.4.1 Hierarchical Control Structure

Control software of SM^2 has been developed for reliable and accurate 3-D locomotion movements on Space Station trusswork. A hierarchical structure of the control system is executed in multiple levels. The system can automatically generate motion specifications, select the control parameters, execute the control, and monitor and display the resulting motions.

The highest level is *full stepping sequence execution* during which the robot walks from an initial configuration to a final configuration on the truss. Using a display menu, Figure 7, we can specify the operating modes and initial and final configurations with respect to the trusswork [4]. The operator may preview model-based animation of the robot's computer-generated route prior to giving the locomotion command. He can then accept or modify the automatically planned route and monitor the robot's progress on the display. During actual locomotion, the robot animation is driven by the robot's joint position sensors.

The next level is *single step motion control* during which one of the node grippers moves from the initial truss node to the final node. The motion can be specified by the higher level, i.e., stepping sequence execution, or by an

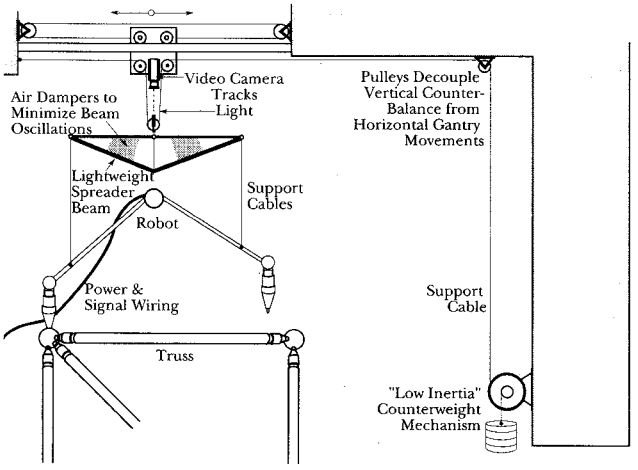

Figure 6: The gravity compensation system simulates zero-gravity for realistic laboratory experiments. A counterweight and cables provide the force to balance the robot, while the support point is servocontrolled to remain above the robot.

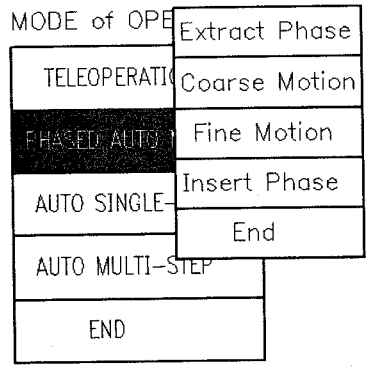

(a)

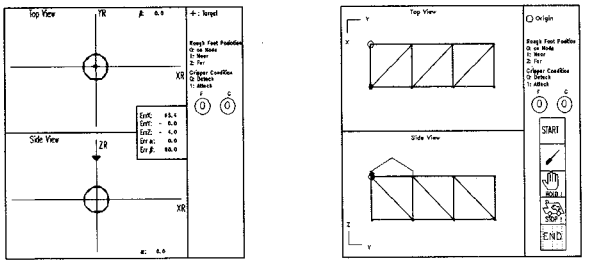

(b)

Figure 7: Screen graphics for the four phases of walking motion. (a) Menu for phase selection. (b) Graphical x-y-z view of robot for fine control (left) and coarse control (right).

operator. As show in Figure 8, each step is decomposed into four phases which are individually tuned for best performance: *extraction* from the initial node, *coarse motion* to the neighborhood of the destination node, *fine motion* to the precise location above the hole, and *insertion* into the node.

One level lower is *single phase motion control* in which a single control law is implemented to optimize the performance in each of the four phases of a step. Here we can specify one of the possible low-level control structures, control parameters, tip motion trajectories, and initial and final locations. Therefore, it is in this level we examine the controllers, trajectories, and performance. Various tip trajectories, such as parabolic and near-optimal trajectories [3], are available for general motion.

The lowest level of the hierarchical structure is *individual joint motion control.* The usage of this level is normally for testing joint controllers, actuating certain joint(s) without involving forward and inverse kinematics for special purposes, or checking sensor readings in each joint.

2.4.2 Multi-Phase Control Strategy

In this section, we discuss in detail the multi-phase control strategy for a single step motion. The 3-D control of SM^2 is a challenge due to its high flexibility, unmodeled joint friction, and positioning errors amplified by the long-reach. The four-phase step decomposition, mentioned above (Figure 8), and shown in block diagram form in Figure 9, allows us to achieve both speed and accurate motion by tuning each phase for optimal performance. In *coarse motion*, a fast and stable motion is desired, and the tracking error from the specified trajectory is not as important as motion efficiency. In *fine motion, extraction* and *insertion* phases stable, precise control, with minimum static error, is the primary concern. Switching between phases is controlled by a *switching mechanism* which depends on the position and velocity errors with respect to the destination.

In *coarse motion*, we implemented a linear joint controller with low integral gains and low-pass filters. The gains of the controllers, and the cut-off frequencies and orders of the filters, are determined by dynamic modal parameters obtained experimentally [7]. The sensor sampling rate is 50 Hz currently. The filter cut-off frequencies are normally set to 2-2.5 Hz to avoid the 3 Hz lateral vibration mode of the elbow joint. The closed-loop frequencies for the first three joints are set to about 1/6 of the filter frequencies, i.e., 1/3 - 1/2 Hz. Using acceleration feedback from the tip, a higher gain can be employed and filter delays can be compensated. A typical PID based, low-level controller is shown in Figure 10. With this controller, the robot is able to execute a 90-degree sweeping step in 5 sec, a 180-degree step in 7 sec.

In *fine motion* and *insertion*, a high gain control is implemented to minimize steady-state error and achieve the precision needed for insertion of the node gripper. Be-

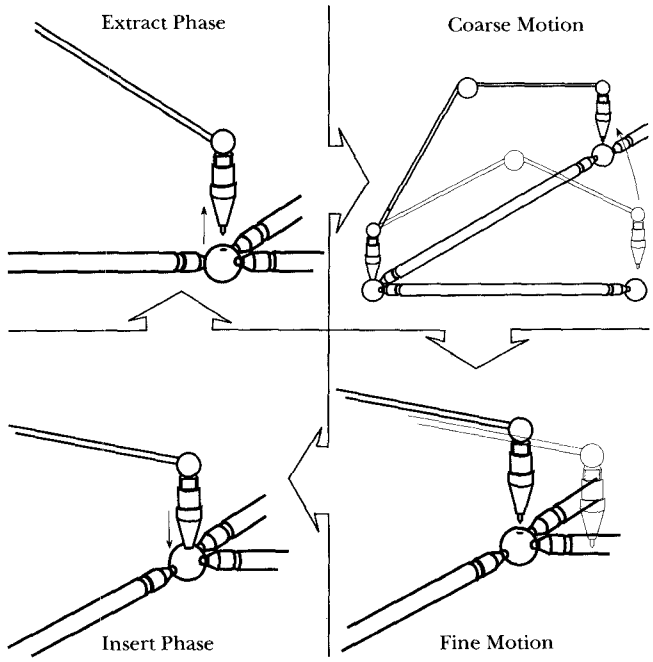

Figure 8: Control of walking motion is divided into four phases, each tuned to optimize performance in that phase.

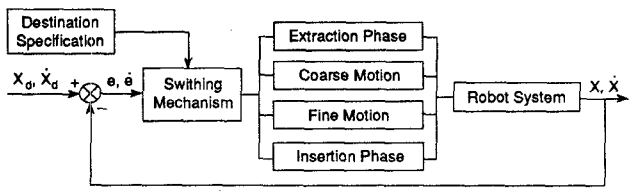

Figure 9: Multi-phase control strategy for single-step motion.

cause motion is relatively small and slow, and thus the deflection of structure will also be small in these phases, a linear structured control with high gains is feasible, and no model-based control scheme is needed. The same control scheme is used for the *extraction* phase.

We found that the use of end-point sensing during the fine motion and insertion phases substantially improved insertion reliablely. A tip-mounted camera provides images of the the node-hole area, which are reduced to 20x24 pixels and processed by a 3-layer, back-propagation neural network [2]. The output of the network consists of two 20-element vectors representing the offsets of the robot's tip relative to the node in the x and y dimensions. The network is trained to generate the appropriate output by correlating several hundred video images with x-y positions measured on a special jig.

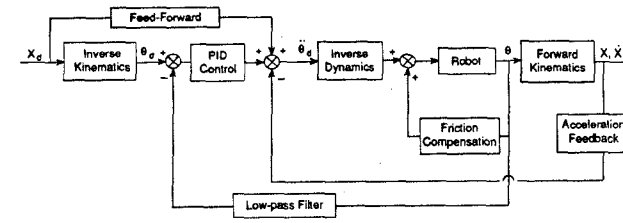

Figure 10: Block diagram of typical PID-based, low-level controller.

2.4.3 Control Hardware

Walking control was implemented on a VME-bus system using an Ironics 68020 CPU running the Chimera II, operating system developed at CMU, communicating with the robot via ADC and DAC boards. Parallel and serial ports allow communication with other processes such as automatic vision. A Sun-3 provides a user interface and program development capability.

3 Manipulation Capability

3.1 Task Evaluation

During the first phase of the project, we developed the basic SM^2 concept, robot hardware, controls, and testbed for walking on the Space Station trusswork. The focus of the second phase of the project is the development of manipulation task capabilities.

A survey conducted at McDonnell Douglas Space Systems Center produced a list of 13 general tasks in which robots on the Space Station could assist in construction, maintenance and inspection. The tasks identified were:

- Fluid line repair;
- Mate/demate quick-disconnects and umbilicals;
- Carry around leak detectors;
- Replace the CETA (Crew and Equipment Translation Aid) cart functions;
- Assist with (truss) segment attachment;
- Deploy radiators;
- Provide high torques;
- Deploy berthing mechanism guides;
- Remove/relocate berthing mechanism covers;
- Fetch tools/ORUs;
- Hold surplus ORUs/tools at worksite;
- Provide additional lighting and camera views; and
- Open airlock/enter airlock.

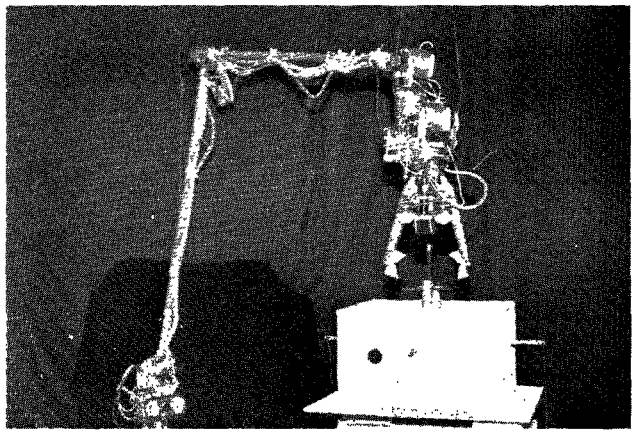

Figure 11: Photograph of SM^2 carrying an ORU mockup.

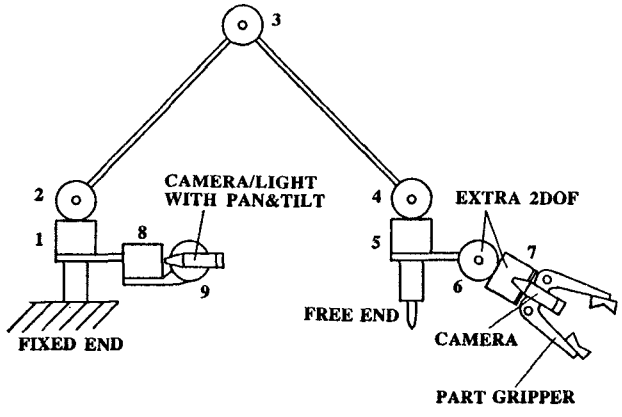

Figure 12: Seven-joint configuration for manipulation.

The majority of the identified tasks can be grouped into one of three general classes:

- Fetch, carry, hold;
- Provide actuating torques or rotations; or
- Position and actuate specialized tools.

The requirements for these tasks are mobility and one-hand positioning abilities that are readily achievable with a simple robot such as SM^2. The five-joint configuration of SM^2 was designed specifically for locomotion, but, with the addition of a sixth DOF, can be exploited to provide manipulation capability.

To develop the task capabilities of SM^2, we selected three general kinds of tasks with increasing levels of sophistication. First were non-contact tasks such as providing lighting and camera views, or carrying sensors, in which loads are minimal and positioning is not critical. Slightly more advanced tasks require some contact with the environment, such as fetching small tools or parts, and delivering these to an astronaut (or another robot). At the highest level are tasks requiring precise manipulation and transport of substantial loads. We have demonstrated the ability of SM^2 to perform tasks at each of these levels, the most sophisticated task being the exchange of an Orbital Replacement Unit (ORU), as shown in Figure 11. Below we describe the hardware and control developments that enabled these task demonstrations.

3.2 Manipulator Configuration

In preparing SM^2 to perform useful work on the Space Station, we extended the hardware to enable manipulation capability. We added two joint modules and a general-purpose gripper (*part gripper*) to one end of the robot, as well as video cameras and lights to aid teleoperation and automatic control. As shown in Figures 12 and 13, this provides a 7-DOF serial configuration for manipulation,

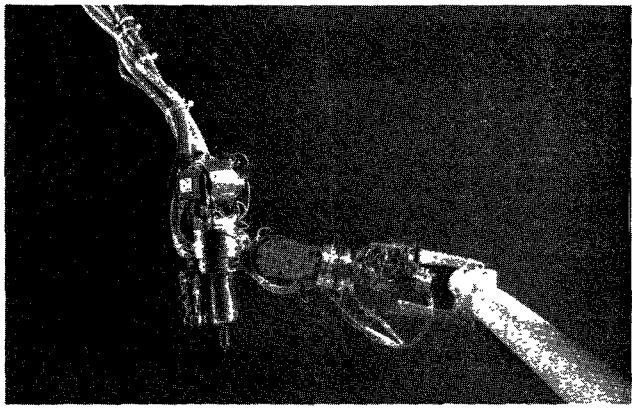

Figure 13: Photograph showing the two joint modules and part gripper added to one end of the robot. Here SM^2 is carrying a long strut.

while the *node gripper* remains available for walking. Thus, for manipulation, the part gripper defines the tip of the robot, while the node gripper at the other end act as the robot's base.

The part gripper was designed specifically for SM^2 and for the kind of tasks we envision. The gripper is electrically actuated, and has V-jaws (each jaw having two orthogonal Vs) suitable for grasping cylindrical or spherical objects from 25 mm (1 in) to 100 mm (4 in) in diameter. The jaws are also compatible with the handle of the ORU mockup that we built, and the gripper contains a motorized hex driver between its jaws to drive the hold-down screw of the ORU mockup. (See Figure 11.) Gripper position (jaw opening) is measured with a potentiometer. Actuator current is measured to provide a rough indication of gripping force.

Vision is provided by two small video cameras at the part gripper (tip) and base node gripper. The tip camera provides a view of objects near the center of the gripper,

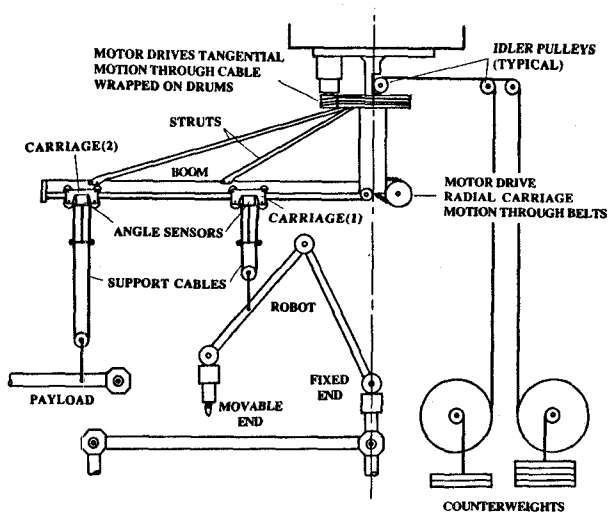

Figure 14: Schematic of the new gravity compensation system (GCII).

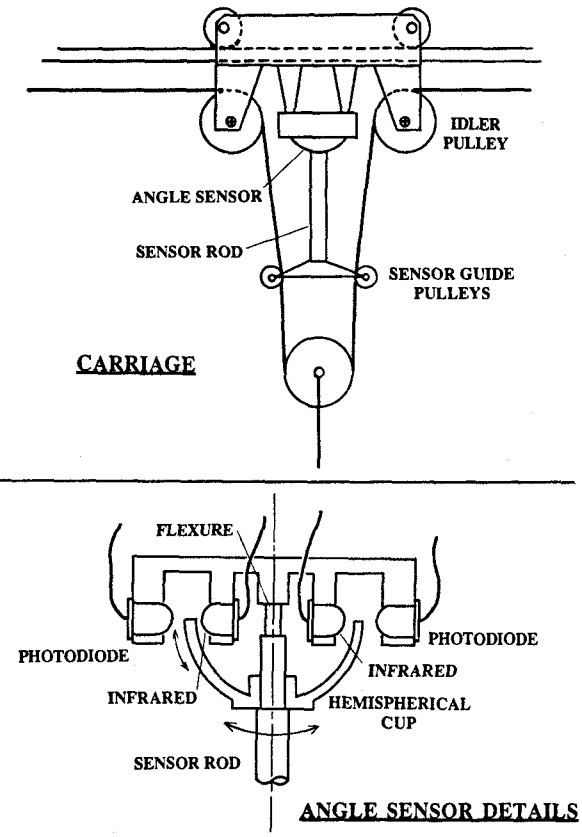

Figure 15: Carriage assembly and cross-sectional view of the angle sensor developed for GCII. The sensor provides precise angle measurements about two axes based on the amount of light received by the photodiodes.

while the base camera, with two additional joint modules for pan and tilt control, can track the robot tip, or be oriented as desired, to provide a second, wider view of the area of interest. Each camera has a pair of high-intensity lamps on either side to illuminate the field of view. A small laser on the gripper centerline provides a light spot that is useful for identifying the relationship between the gripper and target.

3.3 Gravity Compensation System

To facilitate manipulation experiments, we designed and built a second gravity compensation system (GCII). This system, which operates in cylindrical coordinates, has a boom pivoted above the fixed end of the robot, and a carriage that moves along the boom to match the radial movements of the robot, as shown in Figure 14. The second carriage provides a support point for a payload being carried. As with the first system (GCI), GCII has a passive vertical system and an actively controlled horizontal system.

The vertical balancing force is provided for each of the two support points by a 10:1 counterweight mechanism and a system of cables and pulleys. Each support cable runs along the centerline of the boom pivot, along the boom, and through the carriage so that the vertical motion is decoupled from the carriage-radial and boom-swing motions. Rated load capacity is about 14 kg. (30 lb.). Friction in the system causes disturbances to the robot less than 50 gm. (0.1 lb.), 0.3% of the rated capacity.

Horizontal motions are servocontrolled to keep the support point above the robot (or payload). An optical sensor mounted on each carriage (Figure 15). measures the deviation from vertical of the support cable connecting the carriage to the robot. A servocontroller tries to null this deviation by driving motors for the boom swing angle and carriage radial position. A P/D (proportional/derivative) control is implemented in software on a 286 PC, using motors and servoamplifiers from PMI Motion Technologies. Due to its low mass and friction, GCII is fast and precise, and tracks the robot's motions with static errors less 1% (deviation from vertical less than .01 radian), and dynamic errors typically less than 2.5%.

Together the two systems, GCI and GCII, give three independent support points. GCI allows walking experiments where both ends of the robot can be moved. GCII restricts one end of the robot to remain fixed under the boom-pivot point, but provides a second support point for payloads, and the fast and precise motion needed for manipulation and fast-stepping experiments. The two systems can be use together for greater versatility.

3.4 Controls

3.4.1 Control Architecture

To accommodate the manipulation tasks and the new robot configuration, the control software has been upgraded. The 7-joint robot presents a kinematic redundancy which improves manipulation dexterity, but complicates control. We currently constrain the fourth joint to be vertical with respect to the node, assuring the node gripper of the robot will be parallel to the axis of the node hole for insertion. Given this kinematic constraint, the 6-DOF task specification can be mapped into the 7-joint angles. For future comprehensive manipulation tasks, we are looking for a method to automatically generate a kinematic mapping for a redundant robot using a Fuzzy Logic rule base or Neural Network. In this way, we avoid optimization procedures that usually must be carried out in conventional approaches for a given set of conditions, such as time minimization or obstacle avoidance considerations. This approach is appropriate when the environment model is unavailable or the computation is crucial.

We have upgraded the computer hardware to improve performance and provide modularity of functions. Real-time control now runs on *two* Ironics CPUs using Chimera II, one handling mainly I/O processing, the other algorithm execution; this allows faster processing, and separates functions logically. We also have installed a BIT3 bus adapter which controls communication on the VME bus between the real-time processors (Ironics) and host Sun; the Sun now resides in a separate card cage.

3.5 Control Station

While autonomous control is reasonable for locomotion control, teleoperation is an efficient and feasible approach to the control of manipulation in space application. We have developed the teleoperation interface with the *Bird*, a commercial, 6-DOF, free-flying hand controller that provides position and orientation of a radio transmitter (moving) relative to a receiver (stationary). The data are communicated to the real-time robot control computer (Ironics) via a serial line at about 15 Hz. The moving part of the Bird is mounted on a structure that constrains it to 5-DOF (analogous to the 5-joint walker), and holds its position when the controller is released. In addition to the Bird, we have installed a 2-DOF hand controller to control the additional two joints during manipulation operations; a 2-DOF joystick for controlling base-camera pan/tilt, or other functions as programmed; a pair of monitors displaying views from the tip and base cameras; and a set of switches that can be used to control gripper motors, rescaling and reframing of the hand controller and other devices. The overall view of the control station is shown in Figure 16.

Voice control is another dimension of teleoperation. We have implemented a voice recognition system running on a dedicated PC that allows the operator to use voice commands to control manipulation and motion functions, such as gripper closing/opening, node gripper actuation, and rescaling and reframing of hand controller. This allows the operator to keep his hand on the controller and his eyes on the visual displays while performing these operations.

Figure 16: Photograph of the control station used for teleoperation.

The inadequacy of camera views is a general problem in teleoperation. While cameras may provide a reasonable view at the end-effector or other specific areas, the operator often has insufficient information about the overall state of the robot, or configuration of the joints. He may not be aware of imminent collisions of the robot structure, or of approaching singularities or other undesirable configurations. We are developing a graphics system that displays the location of the robot tip relative to its environment (the truss), and shows workspace restrictions, currently the maximum allowable reach. Using this graphics interface, we are also developing a potential field approach to discourage the robot from reaching undesirable configurations.

3.5.1 Adaptive Control

Robot dynamics are significantly affected by changes in both the robot configuration and the payload being carried. We have developed adaptive controllers to deal with both effects.

The inertia and stiffness matrices–i.e. the dynamic behavior–of the flexible robot are highly configuration dependent [7]. To accommodate the inertia and stiffness variations while a simple computed-torque scheme is being used, we implemented a gain-schedule scheme that uses the estimated dynamics, based on joint-angle measurements, to determine the optimal gains of the controller based on a predefined criterion. Using the modal frequencies computed for the current system state, we calculate the gains of the controller as well as the orders and cut-off frequencies of the filters, to maintain the desired performance for

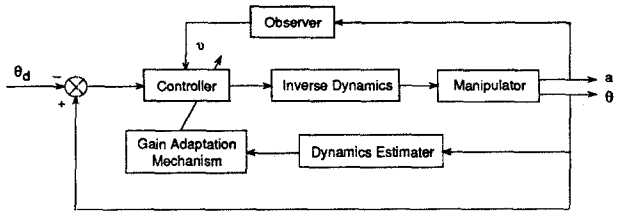

Figure 17: Block diagram of the configuration-independent control scheme based on the gain-schedule approach.

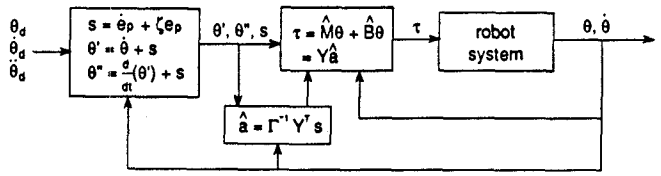

Figure 18: Block diagram of the adaptive control scheme for unknown dynamic parameters. $\hat{\mathbf{M}}$, $\hat{\mathbf{B}}$ and $\hat{\mathbf{a}}$ are the estimated inertia matrix, nonlinear forces, and the set of dynamic parameters to be identified.

all configurations. The block diagram of the controller is shown in Figure 17. A detailed discussion can be found in the paper [5].

To deal with the dynamic changes due to unknown payloads being manipulated or transported, we developed an adaptive control scheme based on the model-reference approach. The algorithm, discussed in detail in our papers [5, 6], and shown in the control block diagram of Figure 18, automatically compensates for uncertainties in position, mass and moments of inertia of a load. The basic idea is to define modified joint velocity and acceleration variables in terms of a composite error function, and use the Lyapunov function approach to guarantee global stability. The experimental results have shown that this algorithm is effective for adapting to unknown masses, allowing stable and precise motion during transport of up to 3 times the mass of the end of the robot. The error in the parameter estimation is less than 30% when the payload is 1/2 the end mass. Compared to other methods, this approach provides an excellent result for both adaptive control and parameter estimation.

4 SM^2 Summary

- General Characteristics:
  - Size: 1.7 meter reach (node-to-node);
  - Mass: 5.2 kg for 7-joint laboratory robot;
  - Configuration: 5-joint walker; 7-joint manipulator; 2-joint base camera holder;
  - Speed: 5 sec per step;
  - Control Station: screen interface, Bird and joystick controllers, voice control interface;
- Capabilities:
  - 3-D walking on trusswork or structured surface;
  - Providing lighting and camera views;
  - Carrying sensors for inspection;
  - Holding, delivering parts and tools;
  - Transport of long strut or other unknown mass;
  - Exchange of Orbital Replacement Unit;
  - Manipulation by teleoperation.

5 Acknowledgements

This work is supported by the Space Projects Office, Shimizu Corporation, Japan. We thank Hiroshi Ueno, Miyuki Ueno, Todd Newton, Nina Zumel, Randy Casciola, Tetsuji Yoshida, John Dolan, Dean Pomerleau, Ju-Jang Lee, and David Stewart for their technical support and contributions.

References

[1] B. Brown, M. Friedman, T. Kanade, and Y. Xu. Self-mobile space manipulator project. *The Robotics Institute Annual Research Review*, 1990.

[2] D. Pomerleau. Neural network based vision for precise control of a walking robot. In *Machine Learning*, 1990.

[3] H. Ueno, Y. Xu, B. Brown, M. Ueno, and T. Kanade. On control and planning of a space station robot walker. In *Proceedings of IEEE Conference on System Engineering*, 1990.

[4] M. Ueno, W. Ross, and M. Friedman. Torcs: A teleoperated robot control system for the self mobile space manipulator. Technical Report CMU-RI-TR-91-07, The Robotics Institute, Carnegie Mellon University, 1991.

[5] Y. Xu, B. Brown, M. Friedman, and T. Kanade. Control system of self-mobile space manipulator. In *(submitted to IEEE Transactions on Robotics and Automation)*, 1991.

[6] Y. Xu, H.Y Shum, J.J. Lee, and T. Kanade. Adaptive control of a space robot system with an attitude controlled base. Technical Report CMU-RI-TR-91-14, The Robotics Institute, Carnegie-Mellon University, 1991.

[7] Y. Xu and H. Ueno. Configuration independent control of self-mobile space manipulator. In *(submitted to Journal of Intelligent and Robotic Systems)*, 1991.